

Parametric optimization of cellular materials through LS-OPT

Alessandro Giustina¹, Ivan Colamartino², Paolo Franzosi, Marco Anghileri¹, Marco Virginio Boniardi²

¹Department of Aerospace Science and Technology, Politecnico di Milano, Via La Masa, 34, Milano, 20156, Italy

²Department of Mechanical Engineering, Politecnico di Milano, Via La Masa, 1, Milano, 20156, Italy

1 Introduction

Cellular materials, characterized by a repetitive pattern of unit cells, feature many advantages with respect to conventional monolithic materials, that make them especially desirable for structural and energy absorption applications.

First of all, the intrinsic cellular architecture, characterized usually by an interconnected network of solid struts and sheets results in a lightweight material [1], which at the same time is able also to dissipate large amounts of energy through the deformation of plastic hinges and local buckling phenomena [2], achieving a superior structural efficiency.

Moreover, some recently developed geometries allowed to achieve highly desirable and unprecedented structural properties, such as negative Poisson's ratio, bistability, or recoverable deformation.

In addition, the recent advancements in additive manufacturing technologies, such as SL (StereoLithography), SLS (Selective Laser Sintering) and MJF (MultiJet Fusion) are now capable of translating intricate geometries, only theorized before, to reality, with remarkable accuracy.

One of the most interesting aspects of cellular materials consists in the possibility of adapting to different materials, loading conditions, and performance requirements by tailoring the geometric parameters. This aspect can be exploited in structural optimizations to create more efficient geometries.

However, the products of Dynamore suite are not able by default to handle optimizations of geometric parameters of cellular materials.

In fact, LS-TaSC[®], its primary topology and shape computation tool, does not allow to create and control cellular structures, with the repetition of base units of cells. Instead, it relies on a density approach, selectively reducing the amount of material where is not needed, without being able to follow the exact geometries of the cells that can lead to specific structural properties of the structure.

On the other hand, LS-OPT[®] application can only interact with parameters defined in LS-DYNA keyword cards and is not able by itself to remesh the model at each iteration. However, the same software LS-OPT[®] has the capability of setting up an optimization problem interfacing with user-defined programs in order to create the input files for LS-DYNA solver.

The aim of our study was to develop custom workflows for the optimization of cellular materials exploiting the LS-OPT[®] interface, for any given parameters, even if not related to any variables specified in LS-DYNA keyword cards.

In this context, external subroutines were implemented in Python environment, allowing to generate and mesh cellular geometries, one for each set of design point parameters, and performing optimization tasks on the performance indexes, given as output responses of the finite element analyses.

The methodology was then applied to three significant case studies of cellular structures for energy absorption applications.

2 Methodology

In order to generate the mesh of the cellular structures it was chosen to use Python codes that could create input files already in .k format, to be run with standard LS-DYNA solvers.

For the simplest geometries, the coordinates of the nodes and element connective matrices were directly written in **#KEYWORD** formats. Geometric parameters can be defined using the following syntax: <<L:6>> in order to be manipulated correctly by LS-OPT®, where L, for example, is the parameter name and the number used is the starting numerical value, although it can be changed directly inside LS-OPT®.

For truss-made intricate structures, external meshing softwares have been used, launched, and run silently by Python commands. In this case, all the necessary keywords essential to the analysis can be written in text format inside .k file or external files and can be included thanks to the specific **#INCLUDE** keyword.

Before being run, the file might need an intermediate Preprocessing stage in order to be properly formatted with respect to the LS-DYNA solver version used and to merge all the parts. Avoiding this step could lead to errors during simulation. The operation is performed by launching silently LS-PrePost using Script Command Language (SCL) methodology through a .lsp file.

The final phase of the sampling stage launches the analyses with the LS-DYNA solver. Subsequently, the results of the simulations are extracted, the metamodel is updated and the cycle starts again.

The block diagram of the optimization workflow is illustrated in fig. 1.

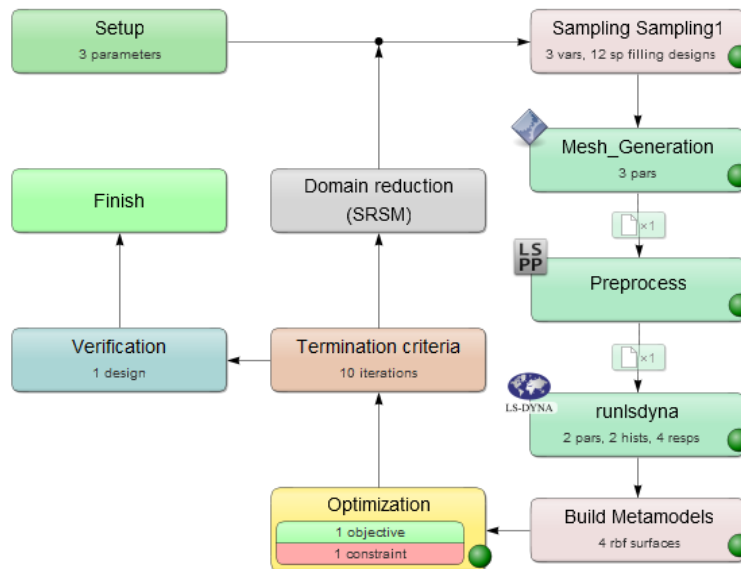


Fig.1: Example of block diagram of the optimization workflow of cellular materials used in the present work

3 Case Studies

The optimization methodology explained in the previous section has been applied to three different case studies of cellular structures for energy absorption applications.

3.1 Negative Stiffness Honeycomb

Negative Stiffness Honeycomb is an arrangement of unit cells made of curved beams, illustrated in fig. 2, with the shape of the first buckling mode with extremities clamped, which, upon transversal loading, exhibits a snap-through behaviour deforming into a second equilibrium position curved in the opposite direction [3].

The deformation results in a region of negative slope in the force-displacement plot and, most interestingly, can be designed to be recoverable, by itself [3,4] or upon external traction [5], allowing to obtain reusable crash absorbers, able to regain functionality after impact and to withstand multiple subsequent collisions.

In the present work, for simplicity, the geometry meshed is composed of one set of double parallel curved beams, modelled with shell elements, as illustrated in fig. 3, while the arrangement of multiple cells is simulated by imposing symmetry boundary conditions with vertical rollers at the extremities of the cell, represented by red triangles in fig. 3.

This modelling strategy allowed to generate the mesh directly in text format .k with Python using the following equation over the length of the beam:

$$w(x) = \frac{h}{2} \left[1 - \cos \left(2\pi \frac{x}{l} \right) \right]$$



Fig.2: Example of Negative Stiffness Honeycomb structure

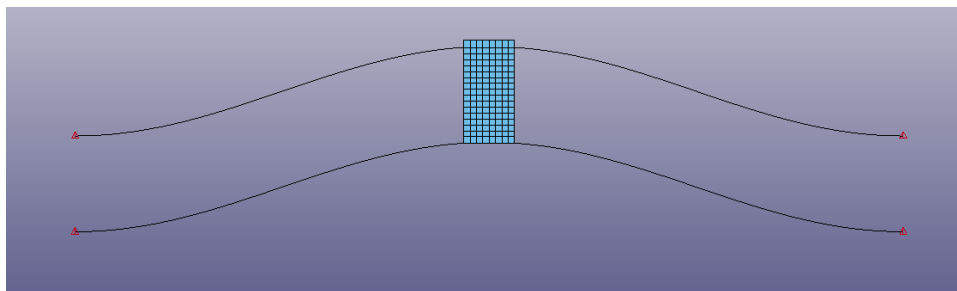


Fig.3: Mesh of Negative stiffness double parallel beam configuration used in the optimization

The parameters of the analysis are shown in fig. 4 and are respectively:

- l: horizontal length of the cell
- h: apex height
- t: thickness of the beams

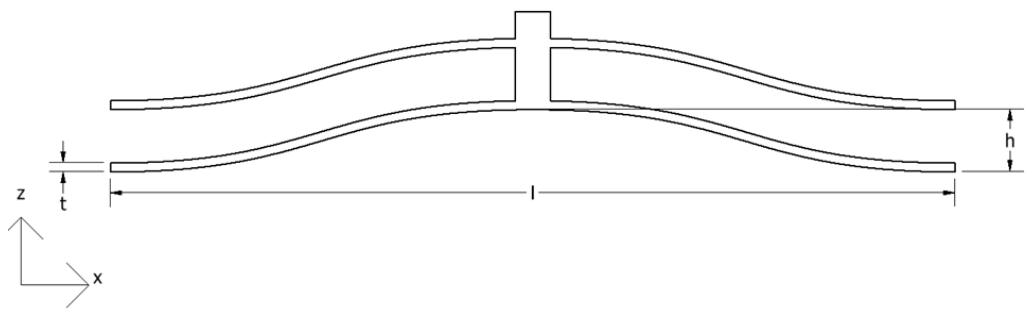


Fig.4: Schematic representation of the parameters used in the optimization

The material chosen for the analysis was stainless steel AISI 304, with full elasto-plastic material modelling. Since the low elastic range of the material, the recoverability of the structure would be enabled by mechanical traction procedure [5]. For this reason, a constraint was imposed to limit the maximum effective plastic strain of the material to 5%.

The mesh selected for the analysis was 1 mm, with only hexahedron solid and tetragonal shell elements used, to ensure reliable results.

The objective function considered was a maximization of the internal energy absorbed by the beams during static compression over the total mass.

In fig. 5 the optimal configuration is shown after 10 iterations, each composed of 12 design points, in comparison with a geometry already developed and experimentally tested internally previously to this work, which obtained the same maximum plastic deformation with the same material, but designed starting instead from analytical formulas.

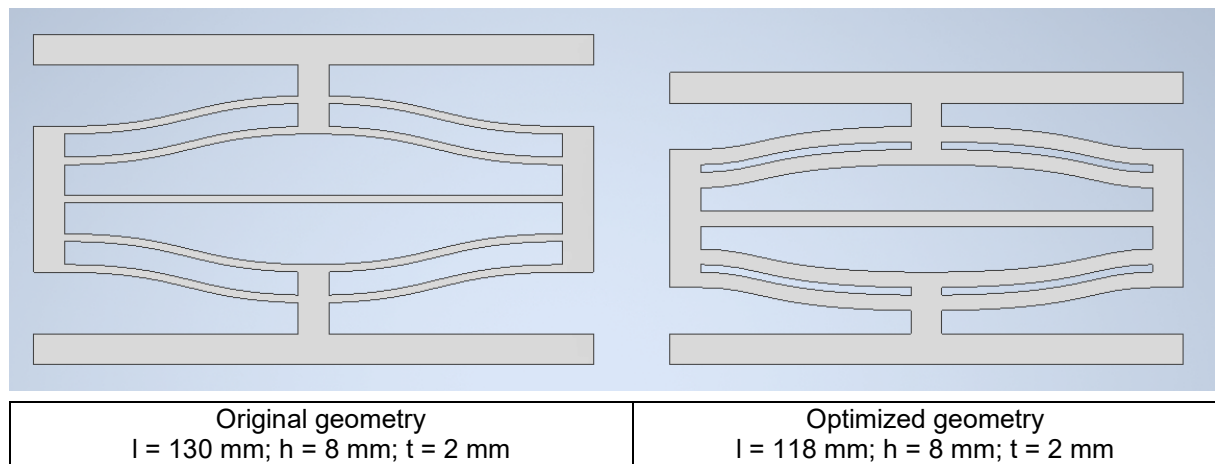


Fig.5: Comparison between original Negative Stiffness Honeycomb cell geometry experimentally tested (left) and optimized geometry after 10 iterations (right)

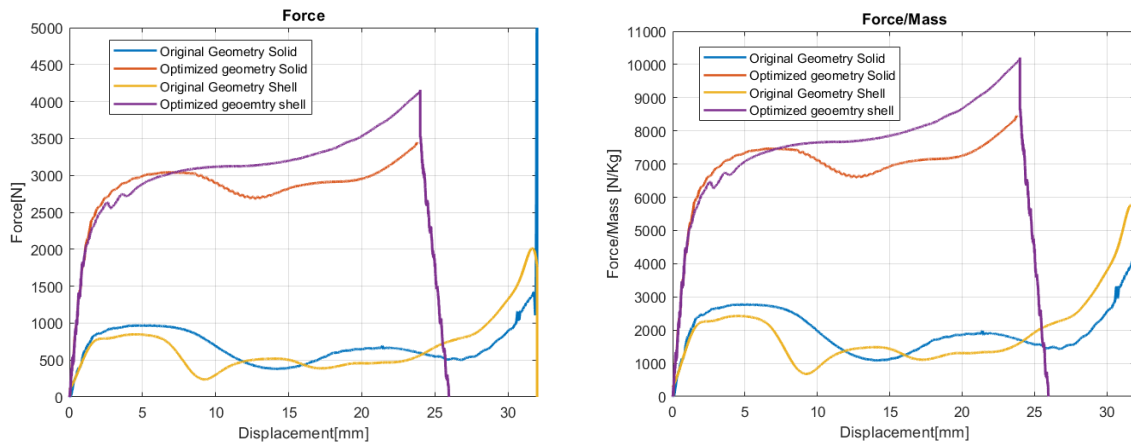


Fig.6: Comparison of Force-Displacement plots of original geometry and optimized geometry of negative stiffness honeycomb cell under static compression

The superiority of the numerical tool is assessed in fig. 6, with an increase with respect to the original geometry of 170% in specific peak force (defined as the peak force during the plateau divided by the mass of the cell) and of 166% regarding the specific energy absorption (computed as the area under the Force-Displacement plot, divided by the mass of the cell). In the plot are also reported the results of simulations performed on cells of the same dimensions but fully modelled with solid elements, in order to prove the accuracy of shell simplification used in the optimization, as explained at the beginning of the paragraph.

3.2 Planar anti-chiral auxetic lattice

Auxetic materials are characterized by a negative Poisson's ratio.

This property has shown promising applications in the fields of impact mitigation and ballistics [6,7], since the material concentrates below the impact area instead of being pushed away, like in conventional structures.

The planar anti-chiral topology has already been proven to be an auxetic structure [8], and in previous internal experimental tests has shown reliable behaviour in dynamic compressions and superior printability exploiting metal laser sintering (SLS), with respect to other auxetic geometries.

In this case, the intricate geometry was generated using external software Gmsh[®], which can be silently run with Python commands, meshed with tetrahedron elements of dimension equal to half of the radius of the struts, following the Frontal-Delaunay algorithm [9], and saved in .key format, in order to be easily read and managed by LS-DYNA.

In the simulations were considered specimens of 20x20mm base, composed of a planar pattern of 4X4 cells, as illustrated in fig. 7. The material selected for the lattice specimens was stainless steel AISI 304, to be manufactured by Selective Laser Sintering.

The parameters considered in the optimization were:

- H: height of the cell
- R: radius of the toroidal element of the cell
- r: radius of the struts

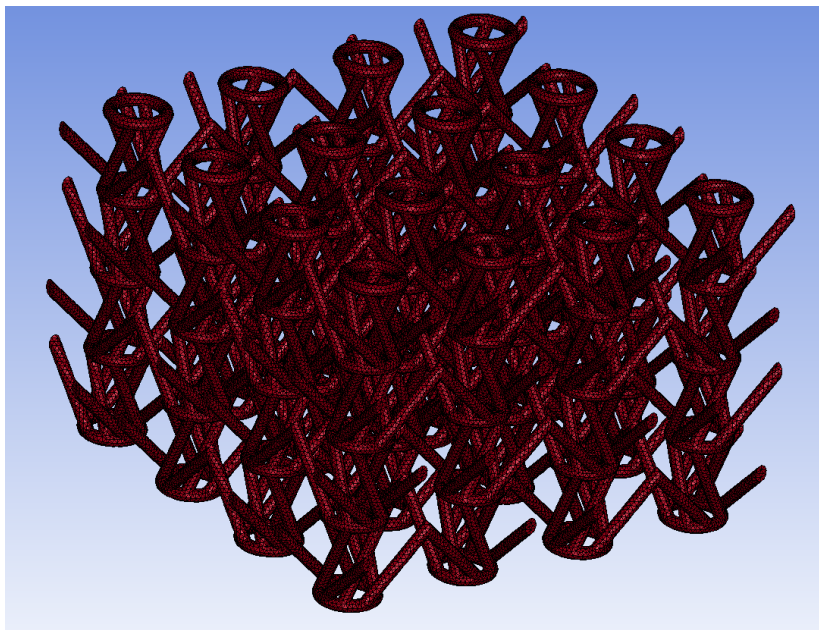


Fig.7: Example of planar anti-chiral auxetic lattice structure meshed in LS-Dyna

Two loading cases have been studied:

- 1) Lattice structures composed of 1 layer of cells, subjected to impact loading with a rigid plate of 100 kg of weight impacting at the initial velocity of 3 m/s. In this case, the objectives evaluated were minimum acceleration peak at full compression and minimum mass. A Pareto optimal front was used to manage the two objectives;
- 2) Lattice structures composed of 2 layers of cells, subjected to static compression. In this case, the only objective of the optimization was a maximization of the energy absorbed up to 30% of full compression over mass (performance parameter which, in the following lines, will be addressed as *specific energy*). This strategy aimed at avoiding instabilities that might arise at full compression of the specimen.

In fig. 8 are illustrated the deformation pattern of the lattice structure and can be effectively observed the negative Poisson behaviour.

Between the horizontal plates and the lattice structure, only friction contact is imposed.

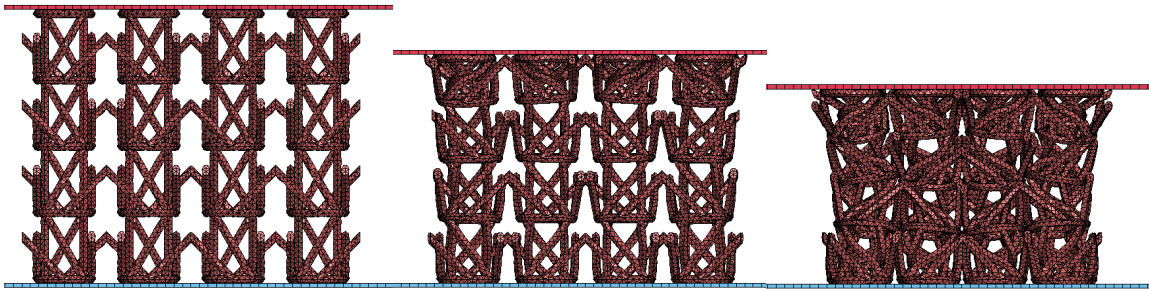


Fig.8: Deformation mechanism of auxetic anti-chiral lattice structure under static compression

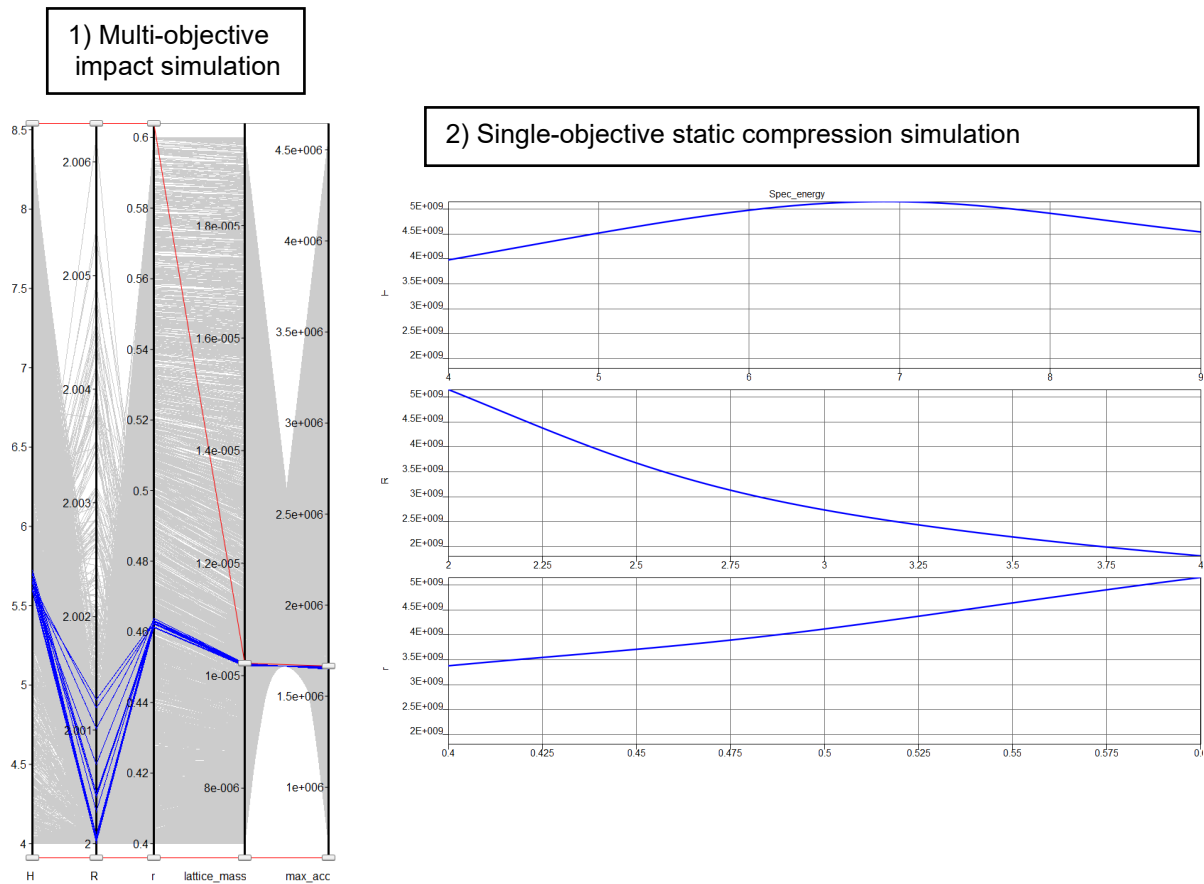


Fig.9: Optimization results of anti-chiral auxetic lattice structures: Multi-objective parallel coordinates results of Pareto optimal solutions in impact tests (left) and influence of geometric parameters on the specific energy of the lattice during static compression (right)

Seven iterations were used in the optimization, each one with 14 design points.

The results of the metamodels of the last iterations of the two loading cases are illustrated in fig. 9 (using Radial Basis Function Network models).

Consistent optimal values of H and R are observed between the two loading cases, with values of H in the range of 5.5 to 7 mm, and low values of R (close to 2 mm). Instead, is observed a difference in the optimal values found for the dimension of the struts in the two loading cases: in the case of the single-objective static compression the specific energy is increasing monotonically with r, instead in the Pareto optimal front for the multi-objective impact case, an optimal value results to be around 0.48 mm.

3.3 Stochastic Voronoi lattice

The stochastic microstructure exhibits a higher degree of isotropy, which might reduce dependence on boundary conditions and improve the structural performance of the lattice [10].

Moreover, irregular porous scaffolds have the ability to simulate the complex microstructures of bone tissues [11] and could have therefore interesting applications in the field of biomechanics and human injury simulations.

In the present work, Voronoi reticula have been generated in open-source software Gmsh[®] starting from random three-dimensional point clouds, subsequently tessellated under the Voronoi scheme and bounded in cuboid shapes.

The mesh was generated in Hypermesh[®] software using the *Shrink Wrap method* [12], with the dimension equal to 1/3 of the diameter of the struts.

In literature is shown the difference between the present type of lattice and other strut-based cellular materials [13].

In the simulations, 40 x 40 x 30 mm specimens (base area x height) have been loaded by penetration with a hemispherical impactor with a diameter of 16 mm.

The material chosen for the specimens in the simulations was Tough2000[®] resin from Formlabs[®], to be manufactured with Stereolithography additive manufacturing technology, numerically modelled with elasto-plastic formulation with included strain-rate dependency.

Four vertical rigid walls were used to restrict the lattice inside a finite volume with contact algorithms and ensure consistent and reliable results, as illustrated in fig. 10.

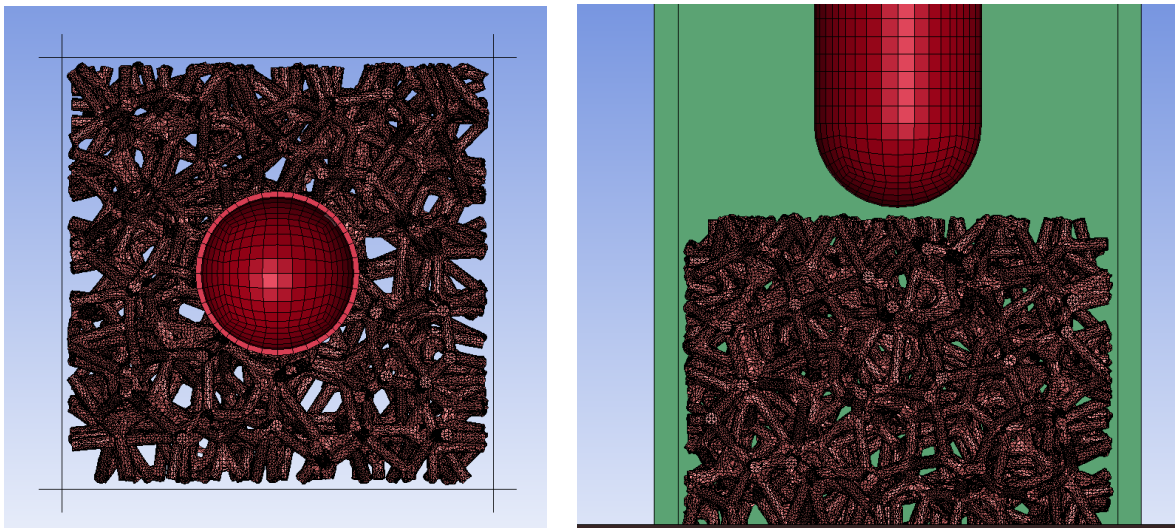


Fig.10: Setup of numerical simulations of Stochastic Voronoi lattices subjected to penetration: top view (left) and frontal view (right)

The geometrical parameters chosen for optimization, univocally defining the Voronoi reticula, were the Poisson minimum distance (λ) for the generation of point clouds and the strut diameter (D). Moreover, was included the possibility of a variation of the parameters with respect to vertical direction with a first-order relation, described as follows, accounting in total for 4 parameters:

$$\begin{aligned}\lambda(z) &= \lambda_0 + \lambda_1 * z \\ D(z) &= D_0 + D_1 * z\end{aligned}$$

In fig. 11 are reported the results of the optimization after 4 iterations of 8 sample points each, using parallel coordinates visualization for Pareto optimal solutions.

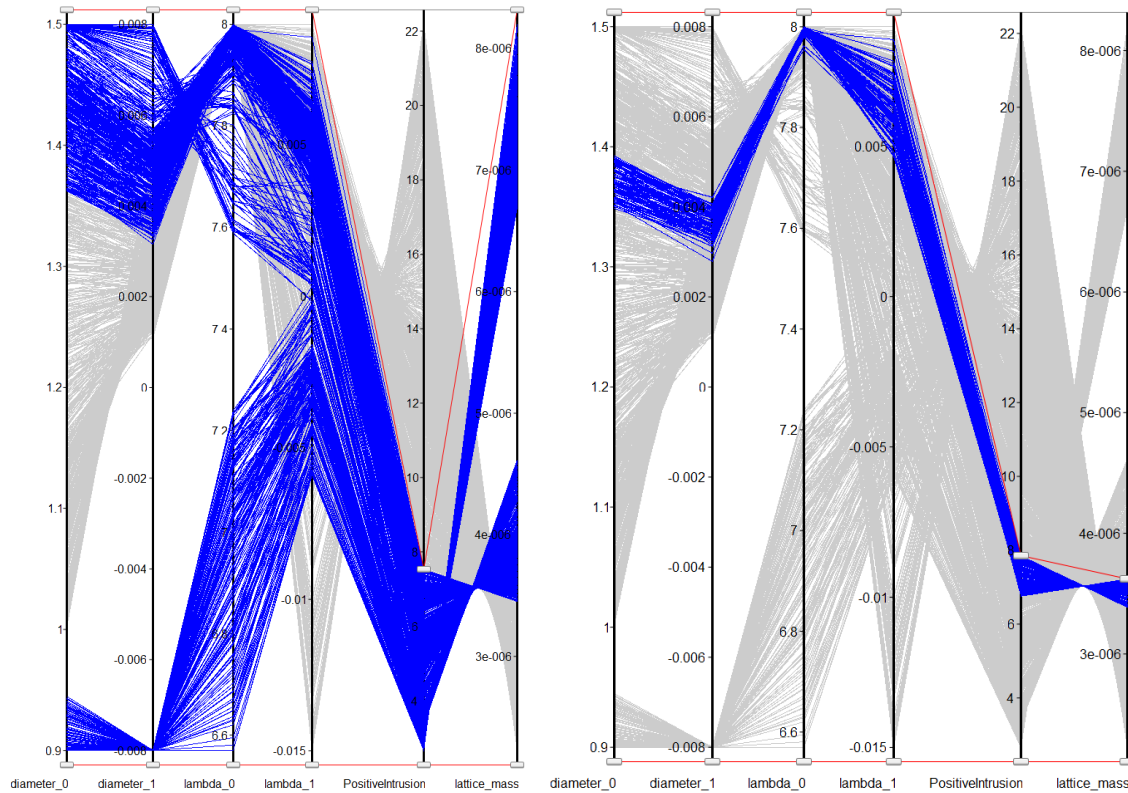


Fig.11: Optimization results of Stochastic Voronoi lattice under penetration with parallel coordinates visualization for Pareto optimal solutions

In particular, it can be observed that low values of penetration can be obtained with two different routes:

- Low initial values of the diameter of the struts and cell dimensions, decreasing in the vertical direction;
- High initial values of both strut diameters and cell dimensions, increasing in vertical direction;

However, the set of values with low length of the cell, hence higher density, results also in higher mass. Consequently, the second strategy ensures the optimal values for balancing resistance to penetration and mass.

4 Conclusions

In the present paper were disclosed original methodologies for solving the problem of geometrical optimization of cellular materials using LS-OPT software. These novel strategies, by us proposed, if adopted, would allow to drastically reduce the design time, performing autonomously a large number of simulations with different characteristic dimensions and selecting the best ones adapting to different performance requirements.

Three case studies of notable cellular structures for energy absorption purposes were investigated (Negative Stiffness Honeycomb, Anti-chiral auxetic lattice, and Stochastic Voronoi lattice), under different loading conditions (static, dynamic compression, and penetration), proving the efficacy and versatility of the proposed methods, and the results are reported together with the respective metamodels.

Advancements can be made considering the possibility of optimizing complex objects with a cellular microstructure continuously instead of considering a representative specimen.

5 Literature

References should be given in the last paragraph of your manuscript. Please use following scheme:

- [1] Novak, N., Plesec, V., Harih, G., Cupar, A., Kaljun, J., & Vesenjaj, M. (2023). Development, fabrication and mechanical characterisation of auxetic bicycle handlebar grip. *Scientific reports*, 13(1), 8158.
- [2] Gibson L. J. (1997), "Cellular solids", Cambridge Solid State Science Series,
- [3] Debeau, D. A., Seepersad, C. C., & Haberman, M. R. (2018) "Impact behavior of negative stiffness honeycomb materials" *Journal of Materials Research*, 33(3), 290-299.
- [4] Gan, J., Li, F., Li, K., Li, E., & Li, B. (2023). "Dynamic failure of 3D printed negative-stiffness meta-sandwich structures under repeated impact loadings". *Composites Science and Technology*, 234, 109928.
- [5] Tan, X., Chen, S., Zhu, S., Wang, B., Xu, P., Yao, K., & Sun, Y. (2019). "Reusable metamaterial via inelastic instability for energy absorption". *International Journal of Mechanical Sciences*, 155, 509-517.
- [6] Yang, S., Qi, C., Wang, D., Gao, R., Hu, H., & Shu, J. (2013)." A comparative study of ballistic resistance of sandwich panels with aluminum foam and auxetic honeycomb cores". *Advances in Mechanical Engineering*, 5, 589216.
- [7] Novak, N., Vesenjaj, M., & Ren, Z. (2016). "Auxetic cellular materials-a review". *Strojniški vestnik- Journal of Mechanical Engineering*, 62(9), 485-493.
- [8] Ebrahimi, H., Mousanezhad, D., Nayeb-Hashemi, H., Norato, J., & Vaziri, A. (2018). "3D cellular metamaterials with planar anti-chiral topology". *Materials & design*, 145, 226-231.
- [9] Geuzaine, C., Remacle, J. F. (2022) , "Gmsh reference manual",
- [10] Chen, L., Fan, Y., Zhang, R., Chu, X., & Liu, H. (2023). "Scale-separated VCUT level set method for designing the graded stochastic Voronoi cellular structure". *Structural and Multidisciplinary Optimization*, 66(3), 54.
- [11] Wang, G., Shen, L., Zhao, J., Liang, H., Xie, D., Tian, Z., & Wang, C. (2018). "Design and compressive behavior of controllable irregular porous scaffolds: Based on voronoi-tessellation and for additive manufacturing". *ACS biomaterials science & engineering*, 4(2), 719-727.
- [12] Altair Engineering, Inc. (2023), "HyperMesh Introduction", HyperWorks 13.0, pag. 279
- [13] Mueller, J., Matlack, K. H., Shea, K., & Daraio, C. (2019). "Energy absorption properties of periodic and stochastic 3D lattice materials". *Advanced Theory and Simulations*, 2(10), 1900081.